Water Research 233 (2023) 119780

Contents lists available at ScienceDirect

Water Research

journal homepage: www.elsevier.com/locate/watres

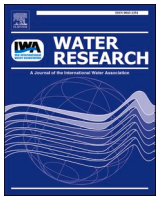

On the importance of temporal floc size statistics and yield strength for population balance equation flocculation model

Jorge A. Penaloza-Giraldo [a,*], Tian-Jian Hsu [a], Andrew J. Manning [a,b,f], Leiping Ye [c], Bernhard Vowinckel [d,e], Eckart Meiburg [e]

[a] Department of Civil and Environmental Engineering, Center for Applied Coastal Research, University of Delaware, Newark, DE 19716, United States
[b] HR Wallingford Ltd, Coasts and Oceans Group, Wallingford OX10 8BA, United Kingdom
[c] School of Marine Sciences, Sun Yat-sen University, Zhuhai, Guangdong 519082, China
[d] Leichtweiß-Institute for Hydraulic Engineering and Water Resources, Technische Universität Braunschweig, Braunschweig, Lower Saxony 38106, Germany
[e] Department of Mechanical Engineering, UC Santa Barbara, Santa Barbara, CA 93106, United States
[f] School of Biological and Marine Sciences, University of Plymouth, Plymouth, Devon, PL4 8AA, United Kingdom

ARTICLE INFO

Keywords:
Flocculation
Population balance equation
Cohesive sediment
Yield strength

ABSTRACT

Many aquatic environments contain cohesive sediments that flocculate and create flocs with a wide range of sizes. The Population Balance Equation (PBE) flocculation model is designed to predict the time-dependent floc size distribution and should be more complete than models based on median floc size. However, a PBE flocculation model includes many empirical parameters to represent important physical, chemical, and biological processes. We report a systematic investigation of key model parameters of the open-source PBE-based size class flocculation model FLOCMOD (Verney, Lafite, Claude Brun-Cottan and Le Hir, 2011) using the measured temporal floc size statistics reported by Keyvani and Strom (2014) at a constant turbulent shear rate S. Results show that the median floc size d_{50}, in terms of both the equilibrium floc size and the initial floc growth, is insufficient to constrain the model parameters. A comprehensive error analysis shows that the model is capable of predicting three floc size statistics d_{16}, d_{50} and d_{84}, which also reveals a clear trend that the best calibrated fragmentation rate (inverse of floc yield strength) is proportional to the floc size statistics considered. Motivated by this finding, the importance of floc yield strength is demonstrated in the predicted temporal evolution of floc size by modeling the floc yield strength as microflocs and macroflocs giving two corresponding fragmentation rates. The model shows a significantly improved agreement in matching the measured floc size statistics.

1. Introduction

Unlike non-cohesive sediment such as sand, cohesive sediments exhibit a unique physical process called flocculation that causes individual particles to stick together when two or more particles collide. Through flocculation, the role of cohesive sediments in aquatic environments has a crucial impact on the ecosystem. When particulate concentrations in the water column are high, aquatic organisms face severe consequences due to the absence of photosynthesis, low levels of dissolved oxygen and depletion of energy sources (Jones et al., 2012; Vaz et al., 2019). Simultaneously, cohesive sediments exert a fundamental control on the fate of nutrients and organic matter and, hence, alter the water quality (Asmala et al., 2022). Furthermore, low-density hydrophobic substances such as oil droplets can be deposited on the seafloor due to flocculation with suspended particulate matters (Daly et al., 2016; Ye et al., 2021). Therefore, studying flocculation dynamics of cohesive sediment is an important and thriving research subject in aquatic science and engineering.

Flocculation is defined by two main processes that coexist simultaneously, aggregation, and fragmentation (breakup). Aggregation may take place when cations from dissolved salt in water create surface bridging around clay particles and decrease their repulsion force (Sutherland et al., 2015). Moreover, cohesion between particles can be significantly increased by bio-cohesion such as extra-cellular polymeric substance (EPS) (Malpezzi et al., 2013; Passow and Alldredge, 1995). For energetic aquatic systems, flow turbulence is considered as the dominant mechanism driving particle collision, which is quantified by the turbulent shear rate (Mhashhash et al., 2018; Spicer and Pratsinis,

* Corresponding author.
E-mail address: japg@udel.edu (J.A. Penaloza-Giraldo).

https://doi.org/10.1016/j.watres.2023.119780
Received 21 October 2022; Received in revised form 12 February 2023; Accepted 20 February 2023
Available online 24 February 2023

1996). This is directly responsible for floc formation and the growth of different floc sizes and their respective densities (porosity; e.g. Lawrence et al., 2022).

Simultaneous with the aggregation process, the flocs can experience a fragmentation (breakup) that decreases their size due to turbulent shear in energetic environments. Flocs can maintain their complex structures up to a specific size because of the floc strength maintained by inter-particle bonds (Bache et al., 1999; Jarvis et al., 2005). The flocs become more fragile as their size increases, and flocs can be broken up when a shear or tensile stress overcomes the floc strength (Yeung and Pelton, 1996). Unfortunately, quantifying the floc strength is not trivial due to difficulties in direct measurement, and a variety of factors, such as mineral types, zeta-potential, floc structures, turbulent shear must be quantified (Jarvis et al., 2005; Sharp et al., 2006; Spencer et al., 2022). Thus, most of the numerical models use a constant value of the floc strength for simplicity (Maggi et al., 2007; Verney et al., 2011; Winterwerp, 1998). In this study, we investigate the limitation of the constant floc yield strength assumption and begin to explore an alternative with satisfactory results.

The single floc size statistic method (Winterwerp, 1998) is usually implemented to track the temporal evolution of the median floc size d_{50}. Although this method has been used in many studies (Kuprenas et al., 2018; Son and Hsu, 2009), it is not designed to represent the complex floc size distribution. On the other hand, the most detailed method is to simulate flocculation using a grain-resolved approach since it tracks all the individual cohesive particles in a fully resolving turbulence field (Vowinckel et al., 2019). This allows to compute the floc strength and the fractal dimension by analyzing the bonds between the primary particles and the floc size/shape. The challenge lies in its limitation to represent practical flocculation problems due to its high computational cost. The middle-ground approaches are to model the floc size distributions. The distribution-based model (Maerz and Wirtz, 2009) requires the assumption of a fixed distribution, which constrains the bimodal floc behaviors observed in aquatic systems (Lee et al., 2011; Manning and Dyer, 2007; Soulsby et al., 2013). This limitation can be overcome by solving Population Balance Equations (PBE) that calculate the number of flocs for each given size class while maintaining the mass balance (Verney et al., 2011; Mietta et al., 2011). Many studies focus on calibrating multiple model parameters in the PBE-based size-class flocculation model using the equilibrium or temporal evolution of median floc size d_{50} (Jeldres et al., 2015; Shen et al., 2018; Zhang et al., 2019), or floc size distribution at the equilibrium state (Coufort et al., 2007). A systematic PBE model calibration was carried out by Mietta et al. (2011) using temporal evolution of the median floc size d_{50} and the equilibrium floc size distribution for a wide variety of compositions (clay type, salt type and different salinity). Importantly, using the temporal evolution of d_{50}, this study showed an inverse proportionality between the collisional efficiency and the zeta-potential. However, it is unclear whether the optimal model parameters can be well constrained by these limited physical quantities.

Motivated by the increasing popularity of PBE flocculation models for cohesive sediment transport applications (Liu et al., 2019; Sherwood et al., 2018), the main goal of this study is to advance the understanding of several key model parameters of the PBE flocculation model and how they determine the resulting temporal evolution of floc size statistics driven by a constant turbulent shear rate. Motivated by the earlier studies on PBE modeling (Verney et al., 2011; Mietta et al., 2011) and floc yield strength (e.g., Jarvis et al., 2005), the specific objectives of this study are to (1) confirm whether the median floc size statistics d_{50}, in terms of both the equilibrium floc size and the initial floc growth, is sufficient to constrain the model parameters, (2) investigate if the model parameters can be better constrained by using the temporal evolution of different floc size statistics, and (3) understand the importance of floc yield strength in the predicted floc size statistics. The remainder of the paper is organized as follows. Section 2 provides a description of the PBE-based size-class flocculation model and the laboratory data used. Section 3 focuses on extensive model investigations and error analyses for predicting the measured data. Section 4 is dedicated to investigating the floc yield strength in the flocculation model and Section 5 concludes this study.

2. Flocculation model description and configuration

2.1. PBE-based size-class flocculation model

The PBE-based size-class flocculation model FLOCMOD (Verney et al., 2011) is adopted to study the physics of flocculation. The model is based on solving PBEs, namely the temporal evolution of the number concentration of each floc size class (i.e., number-based distribution) in a homogeneous isotropic turbulent flow, and it can be written as

$$\frac{dn_k}{dt} = G_{aggr}(k) + G_{break\_shear}(k) - L_{aggr}(k) - L_{break\_shear}(k) \tag{1}$$

where n (unit m^{-3}) is the number concentration (number of flocs per unit volume) of the k^{th} floc size class, t is time (s), G and L with subscripts represent the gain and loss of class k flocs due to aggregation (subscript *aggr*) or breakup induced by turbulent shear stress (subscript *break_shear*). In estuarine and coastal environments, flows are generally energetic, and the model assumes that the turbulent shear is the dominant mechanism driving flocculation. Other aggregation mechanisms resulting from Brownian motion and differential settling are neglected (Maggi et al., 2007). For the low sediment concentration considered in this study, we also neglect the gain and loss of class k due to collision-induced breakup. The gain G_{aggr} and loss L_{aggr} by aggregation are written as

$$G_{aggr}(k) = \frac{1}{2}\sum_{i+j=k} \alpha A(i,j) n_i n_j \tag{2}$$

$$L_{aggr}(k) = \sum_{i=1}^{N} \alpha A(i,k) n_i n_k \tag{3}$$

where A is the two-body collision probability function for spherical particles and α is the collisional efficiency, which parameterizes the sticking properties of flocs and other physical processes not modeled by A (e.g., preferential accumulation that encourages collision or the effect of porosity). This parameter α is assumed constant for the calibration process following Verney et al (2011). Since we assume that the main driving force for flocculation is the turbulent shear, the two-body collision probability function depends on the turbulent shear rate S and the diameters of two colliding flocs, written as

$$A(i,j) = \frac{1}{6} S \left(d_i + d_j\right)^3 \tag{4}$$

where d_i and d_j are the spherical equivalent diameters of two colliding flocs of discrete classes i and j.

The gain G_{break_shear} and loss L_{break_shear} by breakup driven by turbulent shear stress S are defined as

$$G_{break\_shear}(k) = \sum_{i=k+1} FDBS_{ki} B_i n_i \tag{5}$$

$$L_{break\_shear}(k) = B_k n_k \tag{6}$$

where *FDBS* is the distribution function of fragmented flocs representing the gain of daughter flocs from larger floc size classes. Following Verney et al., (2011), we specify the binary distribution assuming that the mass of a floc after breakup is divided in half. The rate at which flocs break due to the turbulent shear rate S is given by the function B, and it is defined as

$$B_i = \beta S^{3/2} d_i \left(\frac{d_i - d_p}{d_p} \right)^{3-f_d} \tag{7}$$

where d_p is the primary particle diameter, f_d is the fractal dimension (Kranenburg, 1994) for equivalent spherical diameter, and β is the fragmentation rate. The fragmentation rate is in fact a dimensional quantity ($s^{1/2} \cdot m^{-1}$) and it is written as (Maggi et al., 2007; Winterwerp, 1998)

$$\beta = E \left(\frac{\mu}{F_y} \right)^{\frac{1}{2}} \tag{8}$$

where μ ($Pa \cdot s$) is the dynamic viscosity of water, E is an empirical (dimensionless) parameter and F_y (N) is the floc yield strength. Although β is a dimensional quantity, it is assumed to be an empirical constant in Verney et al. (2011). This inevitably presumes that the floc yield strength F_y is a constant, which is consistent with the fractal approach (Kranenburg, 1994). Because the direct measurement of floc yield strength is difficult, the assumption of a constant F_y is commonly adopted by many other studies (e.g., Maggi et al., 2007; Wang et al., 2013).

Verney et al. (2011) have pointed out that both the collisional efficiency α and fragmentation rate β are sensitive model parameters that need to be calibrated first with a given cohesive sediment sample. Although the fractal dimension f_d has been estimated from many laboratory and field experiments (e.g., Manning et al., 2010) to be around 2 to 2.5 and there may be a floc size dependency (Khelifa and Hill, 2006; Maggi, 2007) such that larger flocs are more porous and the interparticle bonds are smaller; assuming a constant fractal dimension within a given flocculation experiment remains to be the most practical approach. To successfully calibrate these three empirical parameters concurrently for a given experiment, sufficient information from the measured data is necessary, and a proper calibration strategy may also benefit from a more thorough examination of the governing equations to be solved.

By substituting equations (2) to (6) into the equation (1), the resulting number concentration equation of each floc size class k is written as

$$\frac{dn_k}{dt} = \frac{1}{2} \sum_{i+j=k} \alpha \frac{1}{6} S \left(d_i + d_j \right)^3 n_i n_j + \sum_{i=k+1} FDBS_{ki} \beta S^{3/2} d_i \left(\frac{d_i - d_p}{d_p} \right)^{3-f_d} n_i - \sum_{i=1}^{N} \alpha \frac{1}{6} S \left(d_i + d_j \right)^3 n_i n_k - \beta S^{3/2} d_k \left(\frac{d_k - d_p}{d_p} \right)^{3-f_d} n_k \tag{9}$$

During the initial stage of the flocculation (i.e., floc growth stage), the breakup terms can be neglected (the second and fourth term on the right-hand-side (RHS) of equation (9)) since flocs must grow from small flocs or primary particles and the aggregation terms (first and third terms on the RHS) are dominant. This means that a model calibration focusing on the initial flow growth stage allows us to mainly calibrate α (Mietta et al., 2011). However, beyond the initial floc growth stage, the breakup terms must become important because there must be a balance between aggregation and breakup so that an equilibrium can be reached. Following the analysis presented in Winterwerp (1998), mean equilibrium floc size must depend on the ratio of $r = \alpha / \beta$ and fractal dimension f_d. Therefore, both the equilibrium stage and the initial floc growth stage should be considered for a complete calibration procedure.

Further insights into equilibrium floc size distribution can be gained by setting $dn_k/dt = 0$ in equation (9) which renders an expression for number concentration of each floc size class as

$$n_k = \frac{\left[\frac{1}{12} \frac{r}{S^{1/2}} \sum_{i+j=k} \left(d_i + d_j \right)^3 n_i n_j + \sum_{i=k+1} FDBS_{ki} d_i \left(\frac{d_i - d_p}{d_p} \right)^{3-f_d} n_i \right]}{\left[\frac{1}{6} \frac{r}{S^{1/2}} \sum_{i=1}^{N} \left(d_i + d_j \right)^3 n_i + d_k \left(\frac{d_k - d_p}{d_p} \right)^{3-f_d} \right]} \tag{10}$$

In addition to $r = \alpha/\beta$ and f_d, the breakup distributions functions $FDBS_{ki}$ also control the floc size distribution and must be considered in the calibration. However, the physical evidence of floc breakup distribution function is limited, and most studies assume a binary breakup. Nevertheless, if we focus on very large floc fractions (e.g., macroflocs), their gain due to breakup (G_{break_shear}) and loss due to aggregation (L_{aggr}) can be assumed insignificant compared with the smaller size fraction. Therefore, equation (10) for the very large floc size fraction can be reduced approximately to

$$n_k = \frac{\left[\frac{1}{12} \frac{r}{S^{1/2}} \sum_{i+j=k} \left(d_i + d_j \right)^3 n_i n_j \right]}{\left[d_k \left(\frac{d_k - d_p}{d_p} \right)^{3-f_d} \right]} \tag{11}$$

where the breakup distribution function $FDBS_{ki}$ disappears. Comparing the modeled large floc size statistic with measured data allows calibrating the parameters α, β and f_d with minimum impact of $FDBS_{ki}$. On the other hand, the breakup distribution function $FDBS_{ki}$ must be important for fine floc fractions. Thus, calibrating different size class statistics is valuable, particularly for the coarse floc fraction to avoid uncertainty in $FDBS_{ki}$.

Additional analysis of equation (9) is performed to compare the aggregation and breakup timescales. Following Winterwerp (1998), we estimate the initial floc growth timescale using the aggregation term in the equation (9) and it is written as

$$T_{agg} = \frac{1}{\alpha S \phi_{f,k}} \tag{12}$$

where $\phi_{f,k}$ is the volumetric concentration of floc of size class k. The above expression shows that the collisional efficiency α controls the initial floc growth timescale, and an appropriate calibration process for α should be based on the initial growth time series (Mietta et al., 2011). On the other hand, at the later stage of the floc growth before reaching equilibrium, the floc breakup must play an important role to counteract aggregation. We can examine the breakup timescale as inversely proportional to β and $S^{3/2}$ as

$$T_{brk} \sim \frac{1}{\beta S^{3/2}} \tag{13}$$

For example, to expedite floc growth at the later transient stage, the breakup timescale must be decreased by increasing β (i.e., increase the effect of breakup), which is equivalent to reducing floc yield strength. This point will be revisited in Section 4.

2.2. Experimental data

Keyvani and Strom (2014) report a flocculation experiment in a mixing tank using a mixture of kaolinite and montmorillonite clay. The flocculation experiment was performed for approximately 1800 *min* by using a total sediment mass concentration of $C = 0.05\ kg/m^3$ and a homogeneous turbulence shear rate S of 35 s^{-1}. Hence, the study neglects more complex transport mechanism such as differential advection and settling. Although homogeneous turbulence is highly idealized, it allows a comprehensive calibration of model parameters before the model can be used in conditions with increasing complexity. In addition to the measured median floc diameter d_{50} at equilibrium, Keyvani and Strom (2014) also provide measured temporal evolutions of three different floc size statistics, d_{16}, d_{50} and d_{84} (see Fig. 1) by computing a series of image ensemble every 1 to 5 minute depending on the phase (growth or equilibrium). This comprehensive dataset is selected to calibrate key empirical model parameters in the PBE-based size-class flocculation model of Verney et al. (2011). We simulate three important aspects in the measured time series, the equilibrium state ($t \geq 700$ *min* in Fig. 1), the floc growth stage ($t \leq 200$ *min* in Fig. 1), and the entire time series. In particular, matching the modeled initial floc growth stage with measured data allows us to evaluate the model's ability to predict

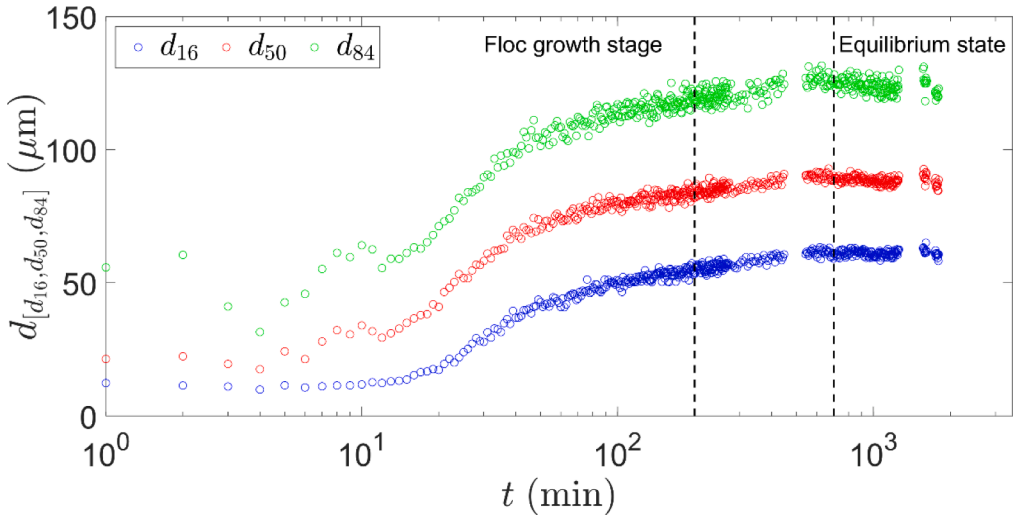

Fig. 1. Measured data reported by Keyvani and Strom (2014) for the temporal evolution of three floc size statistics (d_{16}, d_{50} and d_{84}). The analysis presented here further divides the time series into the initial floc growth stage (initial flocculation rate, $t \leq 200$ min) and the equilibrium state ($t \geq 700$ min).

the flocculation rate, which has been used by other studies to further quantify the stickiness of flocs (Ye et al., 2021) and to calibrate collisional efficiency (Mietta et al., 2011). The abundance of measured data allows a deeper calibration of the model parameters.

2.3. Flocculation model configuration

Following Keyvani and Strom (2014), the total mass concentration and turbulent shear rate from the experiment are prescribed accordingly in the flocculation model. The minimum floc size diameter is established as $d_{\min} = 4\ \mu m$, which corresponds to the diameter of the primary particle typically used for flocculation modeling (Winterwerp, 1998). The maximum floc size is specified to be $d_{\max} = 300\ \mu m$ to ensure the modeled distribution is sufficiently wide and to avoid fluctuations in the distributed mass concentration at the equilibrium state (see Figure S1 in supplementary material). Since Keyvani and Strom (2014) did not discuss the initial floc size distribution, our exploratory numerical experiments show that using a log-normal distribution represents the experimental data better than punctual distribution especially at the early stage of floc growth (see Figure S2 in supplementary material).

Following Verney et al. (2011), an explicit (Euler) time integrator is implemented to solve the PBEs (Equation 1) with an initial time step size equal to 1 s, which is also specified as the maximum allowable time step size throughout the integration. If this value is insufficient to preserve the total sediment mass within a threshold, the time step is decreased by half and the cycle is recomputed until the mass conservation criterion is satisfied. The flocculation model of Verney et al. (2011) requires the use of many classes to discretize the floc diameter distribution. Therefore, establishing the minimum number needed for an accurate numerical solution of the size distribution is an important step. The evaluation is carried out with different numbers of size class N_c to discretize the distribution. Verney et al. (2011) recommended $N_c = 15$ to be sufficient based on calibrating the median floc size d_{50} at the equilibrium state. However, our results suggest that even at $N_c = 25$, the low resolution negatively affects the predicted temporal evolution and, hence, the flocculation rate (see the first 80 minutes of floc growth in Fig. 2a) for fine, median, and coarse fractions. Another issue is the pronounced step-like feature during the floc growth when N_c is small. Careful examination of the model results indicates that the step-like feature is due to coarse numerical discretization of the floc size distribution, but not the time step, (the absence of certain size classes causes a jump in modeled size statistics during floc growth). A converged solution can be obtained when $N_c \geq 75$. In Fig. 2b, we evaluate this convergence by using the Root-Mean-Square-Error *RMSEc* from the target solution using $N_c = 200$. Large errors are observed when $N_c = 15$ especially for the coarse fraction ($RMSEc_{d_{84}} > 40\ \mu m$). By increasing the N_c to 25 and 50, the errors decrease significantly. Our additional numerical experiments suggest that the convergence evaluation is not sensitive to a variation of model parameter of α, β and f_d within a reasonable range. In the rest of the paper, we use $N_c = 75$ to maintain an affordable computational time

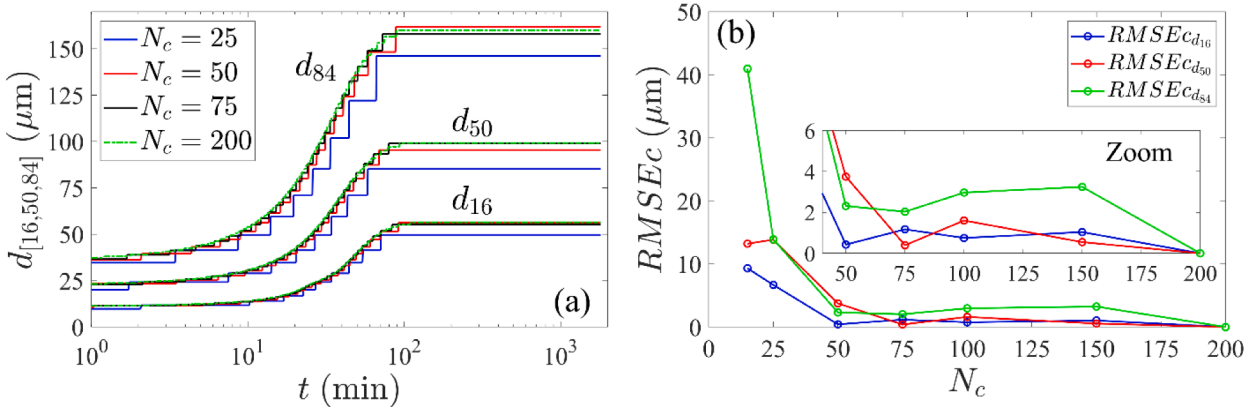

Fig. 2. Convergence analysis for different N_c. (a) Temporal evolution of floc size statistics $d_{[16,\ 50,84]}$ with different number of classes N_c. (b) Root-Mean-Square-Error *RMSEc* for different N_c.

(around 20 minutes per simulation in workstation) with $RMSEc_{d_{[16,50,84]}} \leq 0.5 \sim 3\ \mu m$.

3. Results

Motivated by the previous study of Verney et al. (2011), we concurrently calibrate α and β to match measured data and evaluate if the resulting fractal dimension f_d falls within the expected range. 6,400 simulations were carried out using $\alpha = 5 \times 10^{-2} \sim 80 \times 10^{-2}$ with an interval of 5×10^{-2}, and $\beta = 2 \times 10^{-3} \sim 80 \times 10^{-3}$ with an interval of 2×10^{-3} for ten different fractal dimension values in the range of 1.7 to 2.9. All simulations use a computational time of 1800 *min*. Using the measured data (Keyvani and Strom, 2014) as reference, three different RMSE are computed to evaluate the model performance at the equilibrium state *RMSEeq* ($t \geq 700$ *min*), the growth stage of flocculation *RMSEfr* ($t \leq 200$ *min*), and the entire flocculation time series *RMSEfp* for the tri-temporal floc size statistics d_{16}, d_{50} and d_{84} (see Figures S3~S5 in the Supplemental Material). In Section 3.1 and 3.2, the search for the optimized parameters α, β and f_d is carried out exclusively to match measured d_{50} by these three criteria, namely, minimizing the errors at the equilibrium state $\min(RMSEeq_{d_{50}})$, at the initial growth stage of flocculation $\min(RMSEfr_{d_{50}})$, and for the entire time series $\min(RMSEfp_{d_{50}})$. In Section 3.3, two more criteria are imposed (objective functions) by matching measured fine and coarse fractions, i.e., $\min(RMSEfp_{d_{16}})$ and $\min(RMSEfp_{d_{84}})$.

3.1. Temporal evolution of median floc size d_{50}

The median floc size d_{50} is the most widely reported quantity in laboratory experiments and field observations. We analyze the model's capability to represent the flocculation process using exclusively d_{50} with constraints of the parameters α, β and f_d. Moreover, since many studies only report the median floc size in the equilibrium state, it is important to investigate if the model can reproduce the entire measured time series by solely calibrating model parameters using the equilibrium median floc size.

Using the measured data from Keyvani and Strom (2014) as reference, the RSME at the equilibrium state $RMSEeq_{d_{50}}$ ($t \geq 700$ *min*) is calculated for the 6,400 simulations and results are summarized in Fig. 3 for all combinations of the parameters α, β for any given f_d. Each interaction between these parameters is examined in a simulation with the error magnitudes demarcated by a hot colormap. The dark-red color represents excellent agreement with measured d_{50} in the equilibrium state. Importantly, all the fractal dimensions ($f_d = 1.7 \sim 2.9$) show multiple choices of α and β that are in very good agreement ($RMSEeq_{d_{50}} = 1.72\ \mu m$, the finite value of 1.72 μm reflects the variabilities in the measured data) with the measured d_{50} at the equilibrium state. Clearly, low error values cluster around a line with a constant

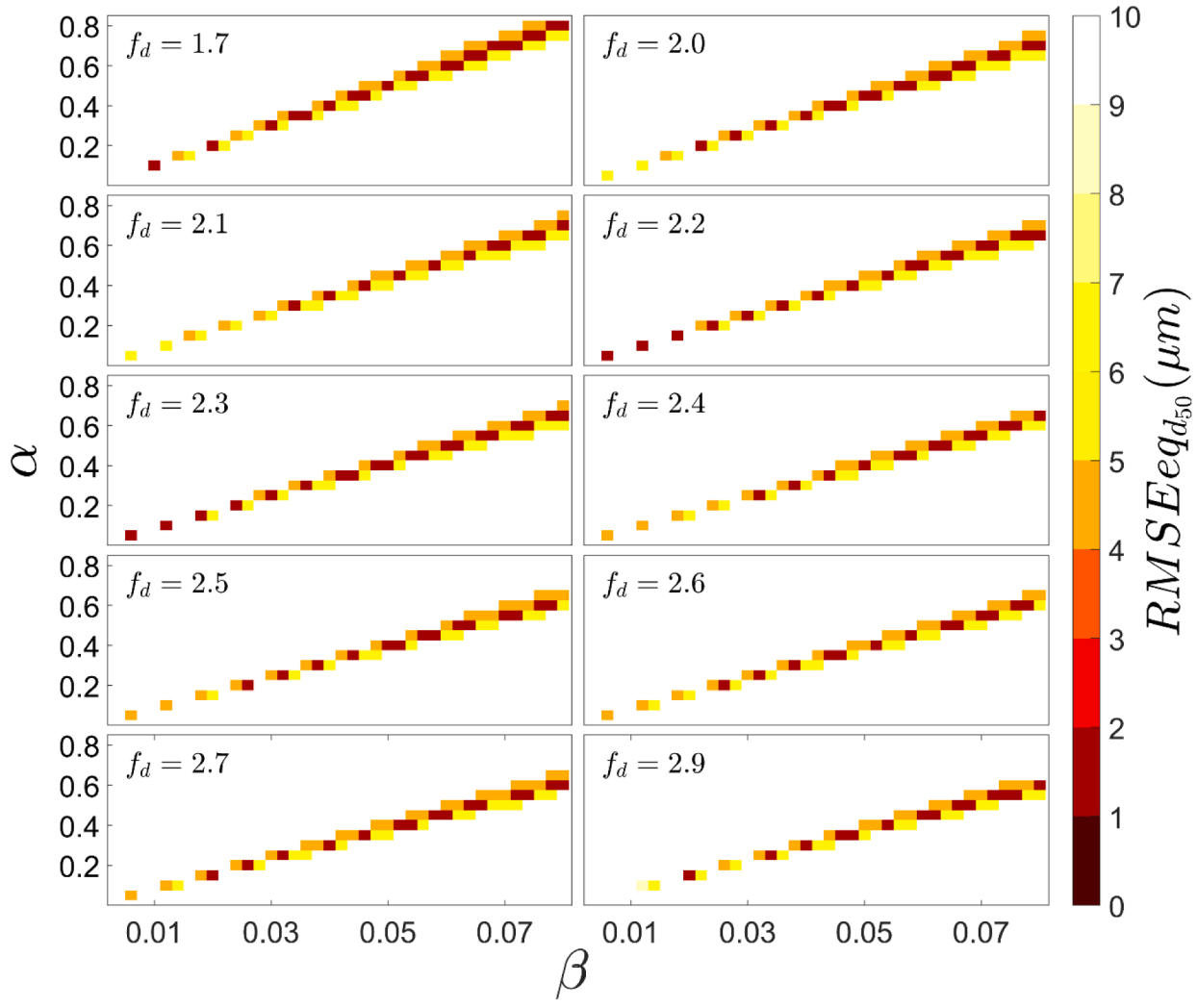

Fig. 3. Root-Mean-Square-Error matrix for the median floc size d_{50} in the equilibrium state for different combinations of collisional efficiency α and fragmentation rate β at fractal dimension f_d from 1.7 to 2.9.

slope for each fractal dimension indicating that the best agreement is obtained at a nearly constant α/β ratio, regardless of the individual α and β values. This finding is consistent with that reported by Verney et al. (2011). In addition to the multiple choices of the α and β pair, another important limitation of using only the equilibrium d_{50} data to calibrate the flocculation model is that excellent agreement can be found for very large (e.g., $f_d = 2.9$) or very low (e.g., $f_d = 1.7$) fractal dimension values outside the typical range for mud. As we will discuss next, despite the multiple options for α and β pairs to match the equilibrium d_{50}, the predicted time series of d_{50} for some of the options are not acceptable (see Fig. 4). At this point, we can conclude that sole measurement of d_{50} in the equilibrium state is insufficient to narrow the values of α, β and f_d. Additional characteristics of the flocculation statistics should be considered for an improved model calibration.

Since there are multiple pairs of α,β values that satisfy minimizing errors in the equilibrium state with min($RMSE_{ed50}$)=1.72 μm, we sequentially applied the second criterion of minimizing the error values at the initial stage of the flocculation ($t \leq 200$ min) min ($RMSEfr_{d50}$). The predicted time series associated with the best and the worst agreement with measured data for the initial stage of flocculation $RMSEfr_{d50}$) are presented for the fractal dimension in the range of $f_d = 1.9 \sim 2.9$ (see Fig. 4). The calibrated parameter values and respective minimum errors at a given fractal dimension are detailed in Table 1. The predicted time series using the pair of α, β that matches the equilibrium d_{50} but having large error of $RMSEfr_{d50}$ are clearly far from satisfactory (see red lines in Fig. 4). This confirms that using solely the first criterion of minimizing the equilibrium median floc size errors is insufficient to predict the entire time series of median floc size evolution. However, applying first the criterion of min $RMSEfr_{d50}$ followed by the second criterion of min $RMSEfr_{d50}$ yields generally good agreement with the measured data for the entire time series when $f_d = 2.2 \sim 2.7$ (see blue lines in Figure 4c~4i) with a $RMSEfr_{d50} \leq 2.8$ μm (see "best" in Table 1). Further analysis confirmed that the same results can be obtained by simply minimizing the errors of the entire flocculation time series, i.e.,

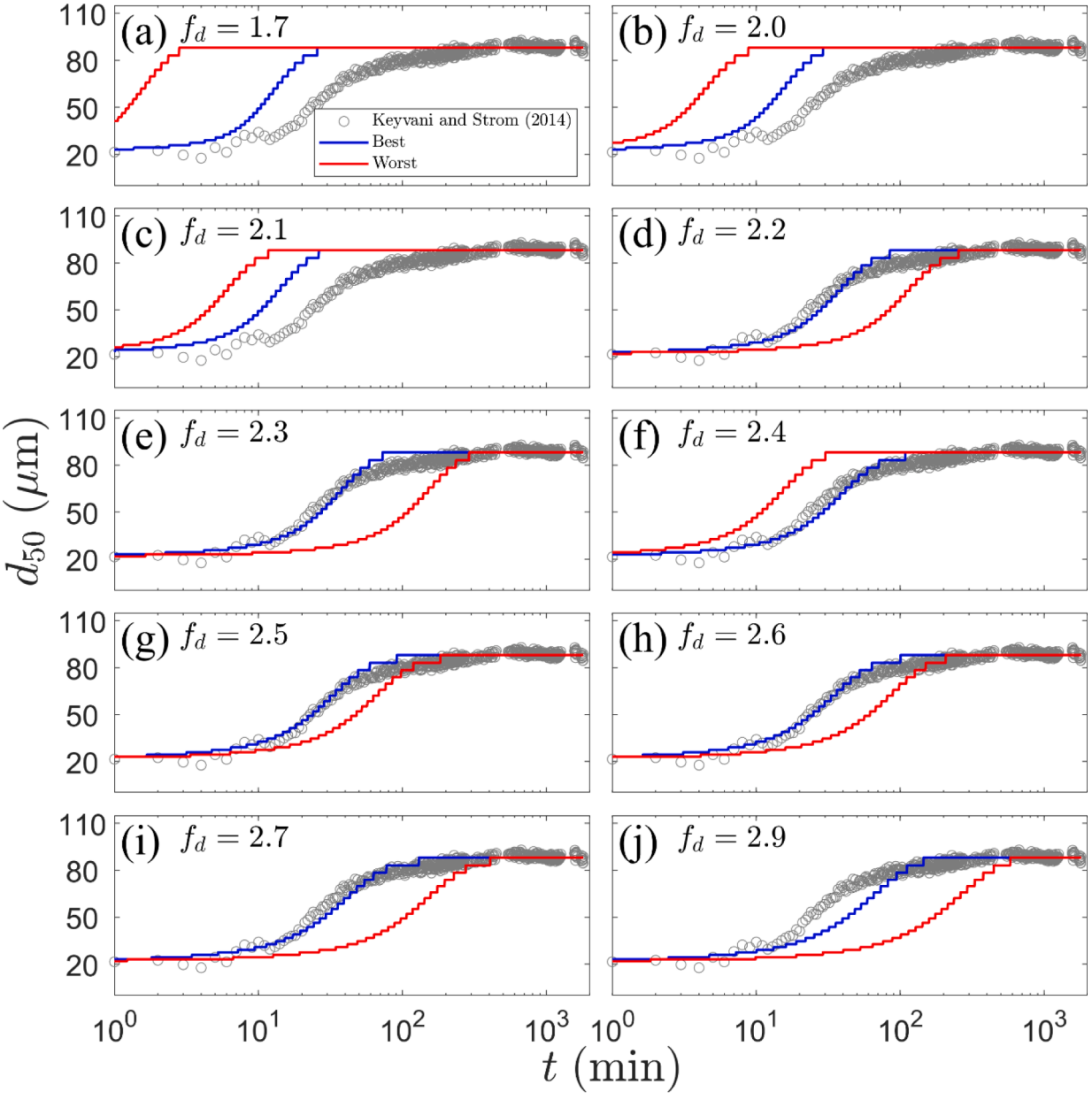

Fig. 4. Temporal evolution of the median floc size d_{50} for different fractal dimension applying the condition min($RMSEeq_{d50}$)→min($RMSEfr_{d50}$) (blue line, best agreement and red line, worst agreement)

Table 1
Root-Mean-Square-Errors (in μm) and flocculation parameters of the median floc size statistics d_{50} obtained in Fig. 4.

	Option	$RMSEeq_{d50}$	$RMSEfr_{d50}$	$RMSEfp_{d50}$	α	β	$r = \alpha/\beta$
1.7	best	1.72	14.58	5.18	0.10	0.010	10.00
	worst	1.72	21.71	7.45	0.80	0.078	10.25
2.0	best	1.72	13.36	4.81	0.20	0.022	9.091
	worst	1.72	19.85	6.85	0.70	0.078	8.974
2.1	best	1.72	14.28	5.09	0.30	0.034	8.824
	worst	1.72	18.93	6.56	0.70	0.080	8.750
2.2	best	1.72	5.98	2.7	0.15	0.018	8.333
	worst	1.72	21.74	7.44	0.05	0.006	8.333
2.3	best	1.72	6.38	2.80	0.20	0.024	8.333
	worst	1.72	27.47	9.35	0.05	0.006	8.333
2.4	best	1.72	5.27	2.54	0.25	0.032	7.813
	worst	1.72	13.58	4.88	0.65	0.080	8.125
2.5	best	1.72	5.76	2.65	0.40	0.052	7.692
	worst	1.72	10.22	3.86	0.20	0.026	7.692
2.6	best	1.72	5.34	2.55	0.50	0.066	7.576
	worst	1.72	14.80	5.25	0.20	0.026	7.692
2.7	best	1.72	4.71	2.41	0.55	0.074	7.432
	worst	1.72	26.72	9.25	0.15	0.020	7.500
2.9	best	1.72	9.13	3.55	0.60	0.080	7.500
	worst	1.72	36.35	13.97	0.15	0.020	7.500

using the objective function min($RMSEfp_{d50}$). Nevertheless, we emphasize our main point that one should proceed with caution when utilizing the equilibrium data as the only model calibration criterion. This result also confirms the importance of matching the flocculation time series to obtain adequate aggregation timescale T_{agg} because it provides a nearly independent data to calibrate α (Mietta et al., 2011).

We further explore the benefits of simply minimizing the errors present at the initial floc growth stage. The best calibrated model parameters and error values can be found in Table 2. As expected, this approach decreases the errors in the predicted flocculation rate (cf. $RMSEfr_{d50}$) in Table 1 and Table 2). The equilibrium state is affected negatively $RMSEeq_{d50}$) values increase from 1.72 μm to 6.06 μm for fractal dimension $f_d = 2.2 \sim 2.7$) but only slightly. Fig. 5 illustrates visually these consequences where the floc growth stage is predicted well but the agreement in the equilibrium value is slightly reduced. This approach also allows us to narrow down the choice of fractal dimension, based on the best three min($RMSEfr_{d50}$, to be $f_d = [2.4,\ 2.5,\ 2.6]$. When evaluating the agreement for the entire time series, we observe that $RMSEfp_{d50}$) is around 5.7 μm for $f_d = [2.4,\ 2.6]$. This is considered good agreement as only one criterion of min $RMSEfr_{d50}$) is adopted. We can also conclude that the PBE-based size class flocculation model has a good capability of predicting equilibrium median floc size once the key model parameters are calibrated for predicting the initial growth of flocculation (i.e., the flocculation rate).

3.2. Tri-temporal floc size statistics using min $RMSEfr_{d50}$)

Since the best calibrated cases that match the measured temporal evolution of median floc size are obtained for a wide range of fractal dimension $f_d = 2.2 \sim 2.7$ (see Fig. 4, $RMSEfp_{d50} \leq 2.8$ μm), the selection of a unique set of $\alpha,\ \beta$ parameters is not yet conclusive. Fortunately, Keyvani and Strom (2014) provide two more measured floc size statistics of d_{16} and d_{84} and these are added to the model calibration to evaluate the possibility of further constraining the model parameters. Fig. 6 illustrates the predicted tri-temporal floc size statistics (d_{50}, d_{16} and d_{84}) at the six fractal dimension values $f_d = 2.2 \sim 2.7$ using the $\alpha,\ \beta$ parameters that achieve the best agreement for the temporal evolution of the median floc size d_{50} (recall Fig. 4). At the initial floc growth stage ($t < 30\ min$), good agreement can be seen for both the fine d_{16} and coarse d_{84} fractions (Fig. 6). However, larger discrepancies arise before reaching the equilibrium stage ($30\ min < t < 200\ min$) for the coarse floc fraction. As discussed before (see equation (13)), this means that the breakup timescale T_{brk} for d_{84} should be reduced (increase the effect of breakup). Moreover, it becomes clear that by minimizing the error for the median floc size d_{50}, the equilibrium floc statistics for the finer fraction d_{16} is under-predicted by the model while the coarse fraction d_{84} is over-predicted.

Identifying the optimum parameters hierarchically to represent the tri-temporal floc size statistics from Fig. 6 can be difficult based on its similar trend across the fractal dimension values. Therefore, we evaluate the error values during the initial growth stage of the flocculation (*RMSEfr*) and the entire flocculation time series (*RMSEfp*) in a wider range of fractal dimension $f_d = 1.7 \sim 2.9$ (see Fig. 7). The *RMSEfr* confirms the discrimination process for the lowest ($f_d \leq 2.1$) and highest ($f_d = 2.9$) fractal dimension since their errors increase considerably. Regarding the fractal dimensions $f_d = 2.2 \sim 2.7$, the *RMSEfr* for the median floc size statistics d_{50} behaves in a quasi-stable way. However, the error values for d_{16} and d_{84} show opposite trends when one of them is minimized (see $f_d = 2.3$ and $f_d = 2.7$). Looking at the average performance for these floc fractions, the first, second and third option are $f_d = 2.7,\ 2.6$ and 2.4, respectively (see dashed black line in Fig. 7a). This result can also be obtained when computing the mean value of *RMSEfp* (see Fig. 7b).

Table 2
Root-Mean-Square-Errors (in μm) and flocculation parameters of the median floc size statistics d_{50} obtained in Fig. 5.

	$RMSEeq_{d50}$ (μm)	$RMSEfr_{d50}$ (μm)	$RMSEfp_{d50}$ (μm)	α	β	$r = \alpha/\beta$
1.7	15.11	6.36	14.25	0.05	0.006	8.33
2.0	6.06	3.16	5.72	0.10	0.010	8.33
2.1	10.70	3.31	10.00	0.15	0.020	7.50
2.2	6.06	2.99	5.71	0.20	0.030	7.69
2.3	6.06	3.25	5.72	0.20	0.030	7.69
2.4	6.06	2.85	5.70	0.30	0.040	7.50
2.5	6.06	2.93	5.70	0.40	0.050	7.41
2.6	6.06	2.49	5.68	0.50	0.070	7.14
2.7	6.06	3.55	5.74	0.55	0.080	7.24
2.9	4.64	8.99	5.50	0.60	0.078	7.69

3.3. Tri-temporal floc size statistics using $\min(RMSEfp_{d_{16}})$ or $\min(RMSEfp_{d_{84}})$

Through a systematic error analysis of d_{50} for the initial floc growth and the entire flocculation process presented in the previous sections, optimal model parameters are obtained. However, the predicted fine (d_{16}) and coarse (d_{84}) floc fractions are adversely affected. That is, better agreement in the fine fraction comes at the expense of worse agreement in the coarse fraction. Now, we evaluate the possibility to narrow the

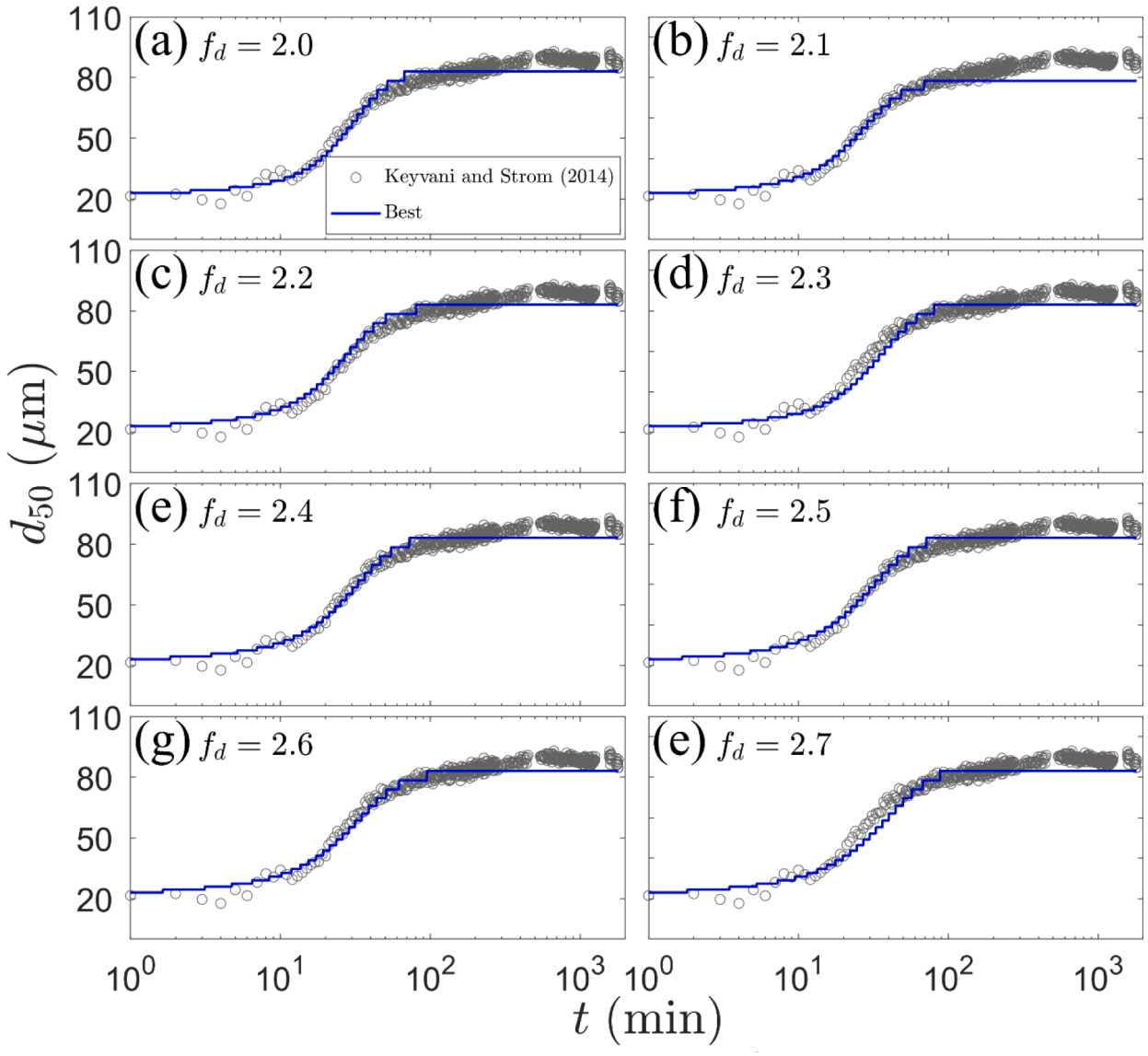

Fig. 5. Temporal evolution of the median floc size statistics d_{50} for different fractal dimension applying the criteria min(RMSEfr$_{d50}$)

flocculation model parameters and improve the overall agreement by minimizing the fine or coarse floc sizes statistic errors (i.e., $\min(RMSEfp_{d_{16}})$ or $\min(RMSEfp_{d_{84}})$) using the same systematic error analysis.

The criterion of minimizing the fine fraction $\min(RMSEfp_{d_{16}})$ produces non-satisfactory results for the overall floc size statistics since the coarse fraction d_{84} stands out for its high error values ($RMSEfp_{d_{84}} \geq 34.62\ \mu m$). This magnitude is higher than $RMSEfp_{d_{84}}$ obtained by using the previous criterion $\min(RMSEfp_{d_{50}})$. Error comparisons are presented in the supplementary material (Figure S6) and they are not further discussed here. Conversely, applying the criterion $\min(RMSEfp_{d_{84}})$ shows satisfactory results especially in the *RMSEfr* values since the best value is distinguished from the other acceptable errors (see $f_d = 2.5$ in Fig. 8a). However, the minimum value of *RMSEfp* averaged over the three size statistics is located at $f_d = 2.9$ (Fig. 8b). This is a limitation in the flocculation model since $f_d = 2.9$ is a much higher than expected value for typical flocs. Considering the error analysis criterion for the initial floc growth stage, the optimum fractal dimension is selected to be $f_d = 2.5$ (see black line in Fig. 8a).

The tri-temporal floc size statistics for three selected cases are presented in Fig. 9. We established previously for the equilibrium state that minimizing the median floc size errors leads to over- and under-predicted results for coarse and fine flocs, respectively (see also Fig. 9a and 9b). Hence, the difference between Case 1 with $f_d = 2.4$ and Case 2 with $f_d = 2.7$ lies mainly in the degree of agreement to represent the coarse fraction d_{84} (see *RMSEeq* values in Table 2) since Case 2 with $f_d = 2.7$ shows 49.12% better agreement compared to Case 1. This contrast can also be noticed in the distributed mass concentration at the equilibrium state (see blue-dashed line vs red-solid line in Fig. 10). Comparing with Case 1, Case 2 relocates a small amount of sediment mass in the coarse fraction to the median and fine fractions due to a relatively larger breakup effect signified by smaller $r = \alpha/\beta = 7.432$ value in Case 2. Using a lower fractal dimension of $f_d = 2.5$ in Case 3 allows for an even lower $r = 6.7$ (i.e., the breakup is stronger in Case 3 than in Case 1 and 2), which significantly reduces the sediment mass in the coarse fraction (see smaller d_{84} in Fig. 9c) and this is evidently due to a more significant relocation of mass from the coarse fraction to the finer fraction (see a shift of sediment mass distribution to the left represented by the black-dashed line in Fig. 10). Case 3 proves the need of increasing the effect of breakup (or lower breakup timescale T_{brk}) for the coarse fraction, which can be achieved by increase the fragmentation rate β. Section 4 investigates this possibility by considering a lower floc yield strength for larger flocs.

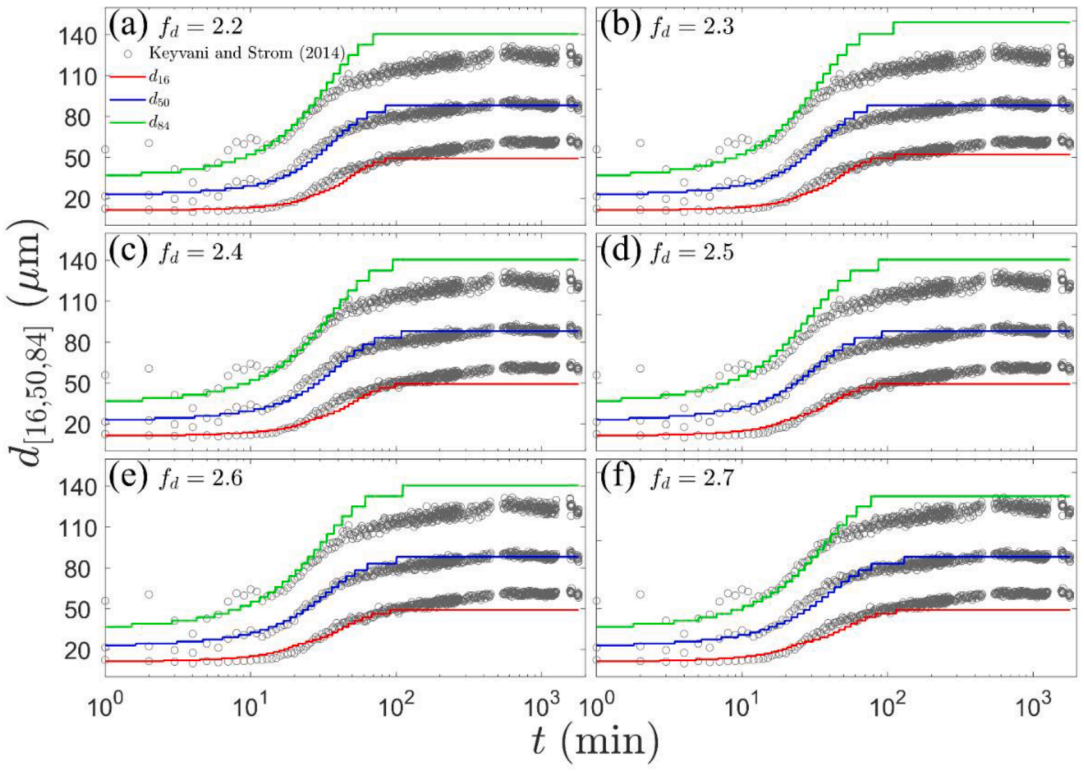

Fig. 6. Temporal evolution of the tri-floc size statistics d_{16}, d_{50} and d_{84} for different fractal dimensions minimizing the entire flocculation process error values $RMSEfp_{d50}$).

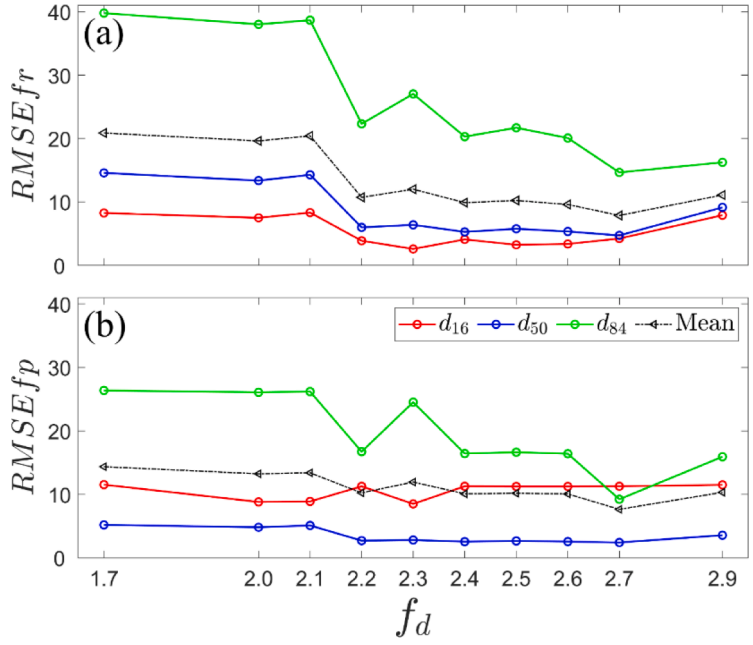

Fig. 7. Root-Mean-Square-Error for tri-temporal floc size statistics (d_{16}, d_{50} and d_{84}) by applying the criterion min $RMSEfp_{d50}$ of minimizing the errors in the measured time series of the median fraction d_{50}. (a) Root-Mean-Square-Error for the growth stage of flocculation (RMSEfr). (b) Root-Mean-Square-Error for the entire temporal evolution (RMSEfp).

4. Discussion - effect of floc yield strength

The results presented in Section 3 indicate that by rigorously calibrating the PBE-based size-class flocculation model against measured tri-temporal floc size statistics (d_{16}, d_{50} and d_{84}), we can identify several combinations of the model parameters (α, β and f_d) that show good agreement with measured data. However, there are still uncertainties in the selection of the best model parameters, particularly in Case 2, which has the best agreement but with a high value of the fractal dimension of 2.7. In this section, we include one other significant physical quantity in the model parameters to improve the overall agreement. To avoid overfitting model results, the choice of the additional physics to be

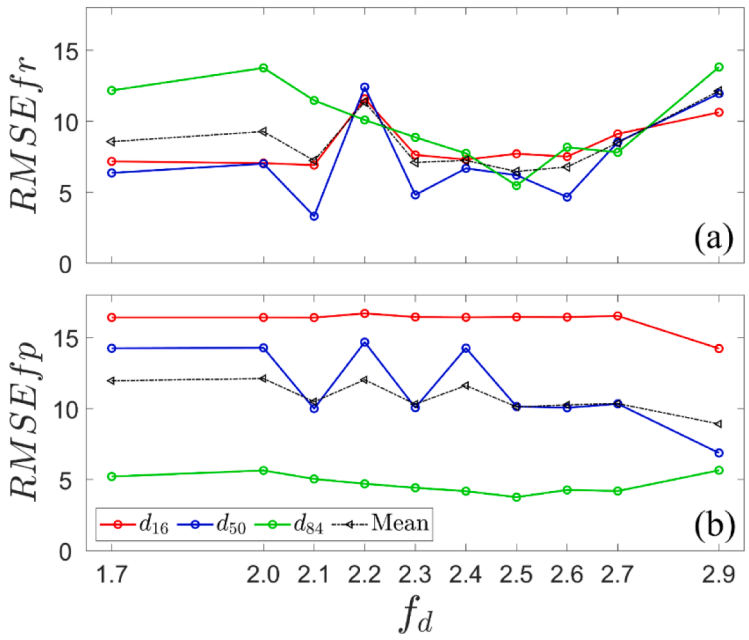

Fig. 8. Root-Mean-Square-Error for tri-temporal floc size statistics by applying min(RMSEfp$_{d84}$). (a) Root-Mean-Square-Error for the initial floc growth stage. (b) Root-Mean-Square-Error for the entire temporal evolution of d_{16}, d_{50} and d_{84}.

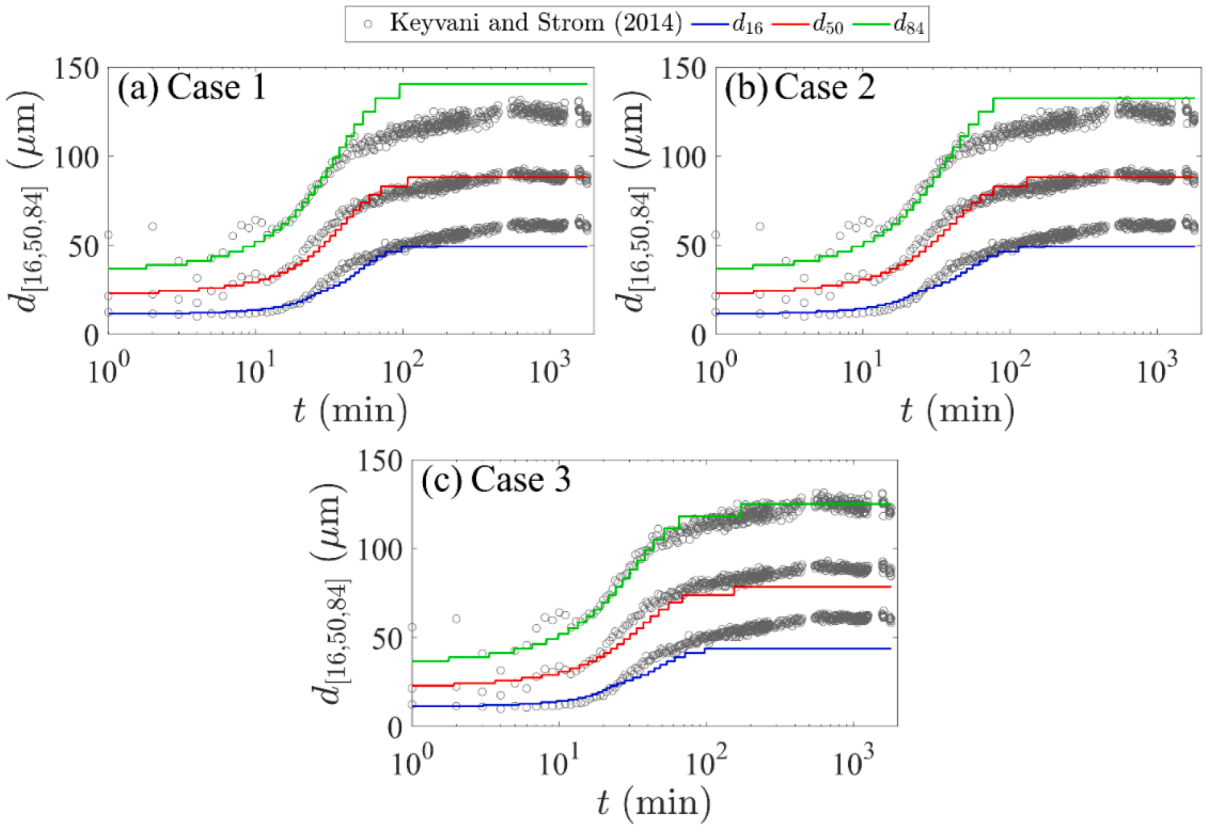

Fig. 9. Modeled tri-temporal floc size statistics (lines) compared with measured data (symbols) reported by Keyvani and Strom (2014). (a) and (b) are Case 1 and Case 2 results using the criteria min($RMSEfp_{d_{50}}$) and (c) Case 3 results using the criterion min($RMSEfp_{d_{84}}$)

included must first be justified.

Motivated by improving the limited capability of the model to represent the coarse and fine fractions simultaneously, and the need to increase floc breakup (or decrease T_{brk}) for the coarse floc fraction, we evaluate the effect of considering the fragmentation rate β as a function of floc size. As shown in equation (8), the fragmentation rate β is a function of the empirical coefficient E, fluid viscosity μ and floc yield strength F_y. The justification of treating β as a constant is to assume the floc yield strength is a constant. In the literature, floc yield strength is routinely assumed to be $F_y = 10^{-10}N$ in flocculation modeling and the

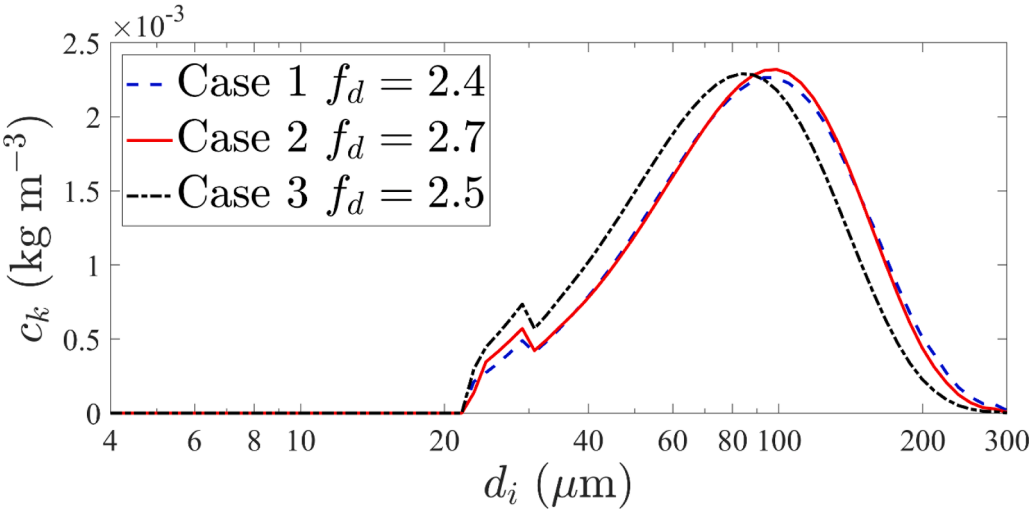

Fig. 10. Distributed mass concentration at the equilibrium state for Case 1 ($f_d = 2.4$) and Case 2 ($f_d = 2.7$) with the criterion min($RMSEfp_{d_{50}}$), and Case 3 ($f_d = 2.5$) with the criterion min($RMSEfp_{d_{84}}$).

model calibrations are carried out either through the coefficient E, or directly using the parameter β (Maggi et al., 2007; Verney et al., 2011; Winterwerp, 1998). However, in the water quality literature, Jarvis et al. (2015) presented a review of many laboratory measurements of floc yield strength (or yield stress) which indicated that the floc yield strength F_y is inversely proportional to the floc size (e.g., Bache et al., 1999; Yeung and Pelton, 1996). In other words, when a floc grows to a sufficient size, the larger the floc size is, the easier the floc can be broken by turbulent shear. This fact is supported by our error analysis presented in Section 3. Fig. 11 presents the best calibrated β values by minimizing the error in the three size fractions (d_{16}, d_{50} and d_{84}) plotted as a function of fractal dimension between 2.3 and 2.6. We observe a clear trend in each fractal dimension that the larger the size fraction when the error is minimized, the larger β (or smaller F_y) is required. Moreover, this trend agrees with the need to decrease the breakup timescale T_{brk} for coarse fraction as has been stated in the previous section. Hence, we investigate the effect of considering the floc yield strength F_y inversely proportional to floc size.

Since measuring the floc yield strength as a function of floc size can be difficult and most studies of cohesive sediment transport do not report such data, as a first step we propose to model the floc yield

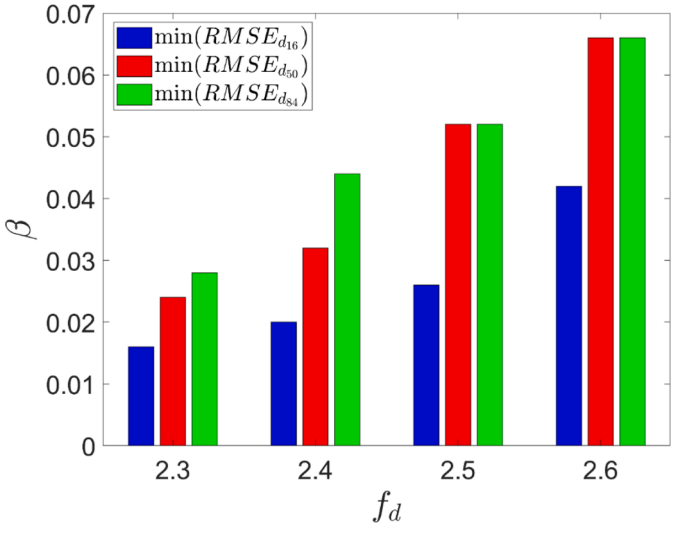

Fig. 11. Fragmentation rate β variation with respect to size fraction based on the criterion min($RMSE_{d_{16,50,84}}$) for fractal dimension $f_d = 2.3 \sim 2.6$.

strength in terms of microflocs and macroflocs (Manning and Dyer, 2007) and divide the fragmentation rate β into two different values accordingly. To distinguish these two groups, a floc size limit d_L is defined such that the fragmentation rate of flocs with a size smaller (larger) than d_L is specified as β_{micro} while the fragmentation rate of flocs larger than d_L is specified as β_{macro}. We investigate the effect of applying the two-value fragmentation rate by simulating Case 1a and Case 3a, which are variants of Case 1 and Case 3 having the same values of α and f_d found in Section 3.2. As for β_{micro} and β_{macro}, the mean value between these two fragmentation rates in Case 1a and Case 3a match with the constant β value used in Case 1 and Case 3, respectively, while satisfying the physical behavior of higher tendency for breakup in macroflocs with $\beta_{\text{macro}} > \beta_{\text{micro}}$.

The use of the two-value $\beta_{\text{micro}}/\beta_{\text{macro}}$ fragmentation rate in Case1a shows a remarkable improvement compared to using a constant β method in Case 1 with $f_d = 2.4$. For the coarse fraction d_{84} under the criterion min($RMSEfp_{d_{50}}$), the over-predicted errors $RMSEfp_{d_{84}}$ for the entire time series in Case 1 (Fig. 12a) are significantly reduced from 16.43 μm to 4.66 μm (nearly a factor 4 reduction of error, compare Table 3 and 4). The same improvement can be seen for the fine fraction d_{16} with an error value $RMSEfp_{d_{16}}$ reducing from 11.27 μm to 3.38 μm. Furthermore, these improvements preserve the excellent agreement of d_{50} because the $RMSEeq_{d_{50}}$ maintains its low error values (errors slightly increase by 5% from 2.54 μm to 2.67 μm). For the floc growth stage, using the two-value $\beta_{\text{micro}}/\beta_{\text{macro}}$ fragmentation rate in Case 1a significantly improves the agreement for the coarse fraction ($RMSEfr_{d_{84}}$ decreases from 20.3 μm to 9.87 μm, about a factor 2 smaller) while only marginally decreasing the agreement for the median (11% increase of error) and fine (42% increase of error) fraction. Evaluating the overall performance through the mean error values, we observe a factor 3 reduction of errors for the entire time series (*mean* ($RMSEfp$) reduces from 10.08 μm to 3.57 μm). The improvement by using the two-value $\beta_{\text{micro}}/\beta_{\text{macro}}$ fragmentation rate is particularly significant for equilibrium floc sizes.

Relatively minor improvement is observed for Case 3a ($f_d = 2.5$, see Table 4) when the two-value fragmentation rate is applied (see Fig. 12b). This is partly because the agreement in the coarse fraction when using a single value β is already good (see Case 3 in Table 3, e.g., $RMSEfp$ for d_{84} is only 3.77 μm). However, the improvement for median fraction and fine fractions by using the two-value fragmentation rate for the entire time series is evident as it is quantified by an error reduction from 10.15 μm to 5.68 μm and from 16.45 μm to 11.3 μm, respectively. As for the floc growth stage, the two-value fragmentation rate also

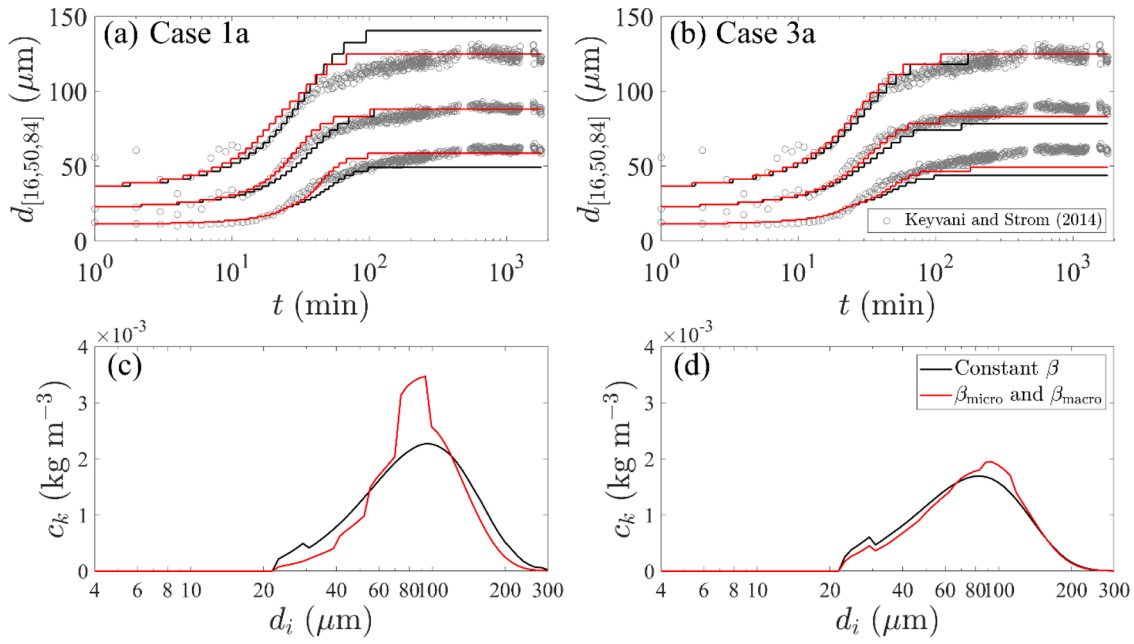

Fig. 12. Comparison between constant fragmentation rate (β) and two-value fragmentation rate (β_{micro} and β_{macro}) for Case 1 and Case 3. (Upper panel) Tri-temporal floc size statistics (d_{16}, d_{50} and d_{84}) based on the (a) criterion $\min(RMSE_{d_{50}})$ and (b) $\min(RMSE_{d_{84}})$. (Lower panel) mass concentration distribution over the floc size classes using the criterion (c) $\min(RMSE_{d_{50}})$ and (d) $\min(RMSE_{d_{84}})$.

Table 3
A summary of recommended cases for their model parameters and errors (in μm).

Case	f_d	d_i	α	β	r	RMSEfr	RMSEfp	mean(RMSEfr)	mean(RMSEfp)
1	2.4	16	0.25	0.032	7.813	4.08	11.27	9.88	10.08
		50				5.27	2.54		
		84				20.30	16.43		
2	2.7	16	0.55	0.074	7.432	4.22	11.27	7.86	7.63
		50				4.71	2.41		
		84				14.65	9.22		
3	2.5	16	0.35	0.052	6.731	7.71	16.45	6.46	10.12
		50				6.20	10.15		
		84				5.47	3.77		

Table 4
A summary of the two-value fragmentation rate cases for their model parameters and errors (in μm).

Case	f_d	d_i	α	β_{micro}	β_{macro}	r	d_L	RMSEfr	*RMSEfp*	mean(RMSEfr)	mean(RMSEfp)
1a	2.4	16	0.25	0.020	0.044	1.95	95.0	5.81	3.38	7.18	3.57
		50						5.85	2.67		
		84						9.87	4.66		
3a	2.5	16	0.35	0.045	0.059	1.68	110.0	4.86	11.30	4.98	7.05
		50						2.47	5.68		
		84						7.60	4.16		

reduces the errors by a factor of about 1.6 and 2.5 for d_{16} and d_{50}, correspondingly. However, the error for the coarse fraction shows a small increase of 39%. A numerical experiment has been carried out for Case 2 with a high fractal dimension of 2.7. We obtain the similar conclusion that the improvement by using a two-value fragmentation rate in Case 2 is very good but not as effective as in Case 1.

The distributed mass concentration at the equilibrium state is another important characteristic that can be used to compare the two-value fragmentation rate approach with the constant β approach (see Fig. 12c and 12d). When the fractal dimension is $f_d = 2.4$, a reduction of the mass concentration in Case 1a is observed for floc classes lower than 55.25 μm and higher than 118 μm (compare the red line with the black line in Fig. 12c). As a result of mass conservation, the mass concentration distribution over the floc size classes is squeezed laterally, and the concentration between the floc classes $55.25 \sim 118$ μm increases. Consequently, the equilibrium floc statistics for coarse d_{84} (fine d_{16}) fraction must decrease (increase). A similar behavior can be seen when the fractal dimension is $f_d = 2.5$ (in Case 3a) but with a different feature. For instance, using a single-value fragmentation rate, the equilibrium floc size for the coarse fraction d_{84} is already in good agreement with measured data. Interestingly, the use of a two-value fragmentation rate effectively decreases the mass concentration in the fine fraction and moves the mass toward the median fraction (Fig. 12d), while the coarse fraction is nearly unchanged. Specifically, the mass concentration increases between $69.77 \sim 157.9$ μm (see Fig. 12d) and decreases in finer fraction ($d_i \leq 69.77$ μm). There is a very small increase of mass concentration in the coarser fraction ($d_i \geq 157.9$ μm).

Conclusion

We present a systematic investigation of the key model parameters for the PBE-based size class flocculation model of Verney et al. (2011) using the experimental data reported by Keyvani and Strom (2014). An analysis on constraining the key model parameters, namely the collisional efficiency, fragmentation rate, and fractal dimension, is first carried out for the median floc size statistics d_{50}. A criterion based on minimizing the equilibrium state median floc size errors provides multiple options of model parameters with many of them misleading since they fail to match the measured initial floc growth. The agreement can be significantly improved by applying a second criterion sequentially minimizing the error for the floc growth stage, or equivalently by minimizing the entire flocculation time series of d_{50}. Interestingly, utilizing the objective function of simply minimizing the error for the floc growth stage ($\min(RMSEfr_{d_{50}})$) shows generally good agreement with the entire measured time series of flocculation, confirming a good predictive ability of the present PBE- flocculation model. The resulting model parameters are constrained to multiple options of fractal dimension in the range of $f_d = 2.2 \sim 2.7$ and we conclude that the median floc size d_{50} alone is insufficient to constrain the flocculation model parameters.

The PBE flocculation model can reasonably predict d_{16} and d_{84} using solely the calibration results from the median floc sizes d_{50} in the range of $f_d = 2.2 \sim 2.7$. The best two options with minimum errors are selected for $f_d = 2.4$ and $f_d = 2.7$ with the latter selected because of its good agreement with measured coarse fraction d_{84} even though the f_d value is higher than expected. Evaluating two different criteria based on minimizing the entire temporal floc size statistic errors of d_{16} and d_{84} indicates that minimizing the errors in the fine fraction is not viable due to the high errors in the coarse fraction. On the contrary, minimizing the error in the coarse fraction shows good agreement with the measured floc growth at $f_d = 2.5$ and suggests that the coarse fraction requires lower breakup timescale (or increased breakup) to balance the aggregation.

To improve the model's predictive ability for fine, median, and coarse fractions at typically expected fractal dimension ranges for cohesive sediment, we propose a two-value fragmentation rate approach (floc yield strength is smaller for macroflocs than microflocs) motivated by limited measured data in the water quality literature and the present model analysis for a single fragmentation rate β, which clearly shows a positive correlation between calibrated β and floc size (see Fig. 11). The results from the two-value fragmentation rate approach demonstrate significant improvement in representing the tri-temporal floc size statistics compared with data from using a constant β, especially for the case of lower fractal dimension at $f_d = 2.4$.

Findings reported in this study are based on modeling the measured three floc size statistics in homogenous turbulence for a single type of clay reported by Keyvani and Strom (2014). Therefore, this work calls for future research on expanding the knowledge of floc yield strength for more diverse configurations. For instance, more laboratory data of temporal floc size distribution for a wide range of turbulence intensity and clay types are needed. Moreover, direct measurements of floc yield strength as a function of floc size are needed. For numerical modeling, coupling the PBE model with a boundary layer sediment transport model to further investigate the role of flocculation dynamics on settling, advection and turbulent suspension of cohesive sediment is warranted.

Authors' contributions

JAPG and TJH: conceptualization, methodology, analysis, and wrote the first draft. AJM, LY, BV and EM: conceptualization, methodology, and revision of the draft.

Declaration of Competing Interest

The authors declare that they have no known competing financial interests or personal relationships that could have appeared to influence the work reported in this paper

Data availability

Data will be made available on request.

Acknowledgment

This research was made possible by grants from National Science Foundation (OCE-1924532, OCE1924655). Authors wish to thank three anonymous reviewers for their insightful comments. Numerical simulations presented in this study were carried out using the Caviness cluster at University of Delaware.

Supplementary materials

Supplementary material associated with this article can be found, in the online version, at doi:10.1016/j.watres.2023.119780.

References

Asmala, E., Virtasalo, J.J., Scheinin, M., Newton, S., Jilbert, T., 2022. Role of particle dynamics in processing of terrestrial nitrogen and phosphorus in the estuarine mixing zone. Limnol. Oceanogr. 67, 1–12. https://doi.org/10.1002/lno.11961.

Bache, D.H., Rasool, E., Moffat, D., McGilligan, F.J., 1999. On the strength and character of alumino-humic flocs. Water Sci. Technol. 40, 81–88. https://doi.org/10.1016/S0273-1223(99)00643-5.

Coufort, C., Bouyer, D., Liné, A., Haut, B., 2007. Modelling of flocculation using a population balance equation. Chem. Eng. Process. Process Intensif. 46, 1264–1273. https://doi.org/10.1016/j.cep.2006.10.012.

Daly, K.L., Passow, U., Chanton, J., Hollander, D., 2016. Assessing the impacts of oil-associated marine snow formation and sedimentation during and after the Deepwater Horizon oil spill. Anthropocene 13, 18–33. https://doi.org/10.1016/j.ancene.2016.01.006.

Lawrence, T.J., Carr, S.J., Wheatland, J.A.T., Manning, A.J., Spencer, K.L., 2022. Quantifying the 3D structure and function of porosity and pore space in natural sediment flocs. J. Sedim. Soils 22, 3176–3188. https://doi.org/10.1007/s11368-022-03304-x.

Jarvis, P., Jefferson, B., Gregory, J., Parsons, S.A., 2005. A review of floc strength and breakage. Water Res. 39, 3121–3137. https://doi.org/10.1016/j.watres.2005.05.022.

Jeldres, R.I., Concha, F., Toledo, P.G., 2015. Population balance modelling of particle flocculation with attention to aggregate restructuring and permeability. Adv. Colloid Interface Sci. 224, 62–71. https://doi.org/10.1016/j.cis.2015.07.009.

Jones, J.I., Murphy, J.F., Collins, A.L., Sear, D.A., Naden, P.S., Armitage, P.D., 2012. The impact of fine sediment on macro-invertebrates. River Res. Appl. 28, 1055–1071. https://doi.org/10.1002/rra.1516.

Keyvani, A., Strom, K., 2014. Influence of cycles of high and low turbulent shear on the growth rate and equilibrium size of mud flocs. Mar. Geol. https://doi.org/10.1016/j.margeo.2014.04.010.

Khelifa, A., Hill, P.S., 2006. Models for effective density and settling velocity of flocs. J. Hydraul. Res. 44, 390–401. https://doi.org/10.1080/00221686.2006.9521690.

Kranenburg, C., 1994. The fractal structure of cohesive sediment aggregates. Estuar. Coast. Shelf Sci. 39, 451–460. https://doi.org/10.1006/ecss.1994.1075.

Kuprenas, R., Tran, D., Strom, K., 2018. A shear-limited flocculation model for dynamically predicting average floc size. J. Geophys. Res. Ocean. 123, 6736–6752. https://doi.org/10.1029/2018JC014154.

Lee, B.J., Toorman, E., Molz, F.J., Wang, J., 2011. A two-class population balance equation yielding bimodal flocculation of marine or estuarine sediments. Water Res. 45, 2131–2145. https://doi.org/10.1016/j.watres.2010.12.028.

Liu, J., Liang, J.-H., Xu, K., Chen, Q., Ozdemir, C.E., 2019. Modeling sediment flocculation in langmuir turbulence. J. Geophys. Res. Ocean. 124, 7883–7907. https://doi.org/10.1029/2019JC015197.

Maerz, J., Wirtz, K., 2009. Resolving physically and biologically driven suspended particulate matter dynamics in a tidal basin with a distribution-based model. Estuar. Coast. Shelf Sci. 84, 128–138. https://doi.org/10.1016/j.ecss.2009.05.015.

Maggi, F., 2007. Variable fractal dimension: A major control for floc structure and flocculation kinematics of suspended cohesive sediment. J. Geophys. Res. Ocean. 112 https://doi.org/10.1029/2006JC003951.

Maggi, F., Mietta, F., Winterwerp, J.C., 2007. Effect of variable fractal dimension on the floc size distribution of suspended cohesive sediment. J. Hydrol. 343, 43–55. https://doi.org/10.1016/J.JHYDROL.2007.05.035.

Malpezzi, M.A., Sanford, L.P., Crump, B.C., 2013. Abundance and distribution of transparent exopolymer particles in the estuarine turbidity maximum of Chesapeake Bay. Mar. Ecol. Prog. Ser. 486, 23–35.

Manning, A.J., Baugh, J.V, Spearman, J.R., Whitehouse, R.J.S., 2010. Flocculation settling characteristics of mud: sand mixtures. Ocean Dyn. 60, 237–253. https://doi.org/10.1007/s10236-009-0251-0.

Manning, A.J., Dyer, K.R., 2007. Mass settling flux of fine sediments in Northern European estuaries: measurements and predictions. Mar. Geol. 245, 107–122. https://doi.org/10.1016/j.margeo.2007.07.005.

Mhashhash, A., Bockelmann-Evans, B., Pan, S., 2018. Effect of hydrodynamics factors on sediment flocculation processes in estuaries. J. Soils Sediments 18, 3094–3103. https://doi.org/10.1007/s11368-017-1837-7.

Mietta, F., Chassagne, C., Verney, R., Winterwerp, J.C., 2011. On the behavior of mud floc size distribution: model calibration and model behavior. Ocean Dyn 61, 257–271. https://doi.org/10.1007/s10236-010-0330-2.

Passow, U., Alldredge, A.L., 1995. Aggregation of a diatom bloom in a mesocosm: the role of transparent exopolymer particles (TEP). Deep Sea Res. Part II Top. Stud. Oceanogr. 42, 99–109. https://doi.org/10.1016/0967-0645(95)00006-C.

Sharp, E.L., Jarvis, P., Parsons, S.A., Jefferson, B., 2006. The impact of zeta potential on the physical properties of ferric−NOM flocs. Environ. Sci. Technol. 40, 3934–3940. https://doi.org/10.1021/es051919r.

Shen, X., Lee, B.J., Fettweis, M., Toorman, E.A., 2018. A tri-modal flocculation model coupled with TELEMAC for estuarine muds both in the laboratory and in the field. Water Res 145, 473–486. https://doi.org/10.1016/J.WATRES.2018.08.062.

Sherwood, C.R., Aretxabaleta, A.L., Harris, C.K., Rinehimer, J.P., Verney, R., Ferré, B., 2018. Cohesive and mixed sediment in the Regional Ocean Modeling System (ROMS v3.6) implemented in the Coupled Ocean–Atmosphere–Wave–Sediment Transport Modeling System (COAWST r1234). Geosci. Model Dev. 11, 1849–1871. https://doi.org/10.5194/gmd-11-1849-2018.

Son, M., Hsu, T.-J., 2009. The effect of variable yield strength and variable fractal dimension on flocculation of cohesive sediment. Water Res 43, 3582–3592. https://doi.org/10.1016/j.watres.2009.05.016.

Spicer, P.T., Pratsinis, S.E., 1996. Shear-induced flocculation: The evolution of floc structure and the shape of the size distribution at steady state. Water Res 30, 1049–1056. https://doi.org/10.1016/0043-1354(95)00253-7.

Soulsby, R.L., Manning, A.J., Spearman, J., Whitehouse, R.J.S., 2013. Settling velocity and mass settling flux of flocculated estuarine sediments. Marine Geology. https://doi.org/10.1016/j.margeo.2013.04.006.

Spencer, K.L., Wheatland, J.A.T., Carr, S.J., Manning, A.J., Bushby, A.J., Gua, C., Botto, L., Lawrence, T., 2022. Quantification of 3-dimensional structure and properties of flocculated natural suspended sediment. Water Research, Volume 222, 118835. https://doi.org/10.1016/j.watres.2022.118835.

Sutherland, B.R., Barrett, K.J., Gingras, M.K., 2015. Clay settling in fresh and salt water. Environ. Fluid Mech. 15, 147–160. https://doi.org/10.1007/s10652-014-9365-0.

Vaz, N., Vaz, L., Serôdio, J., Dias, J.M., 2019. A modeling study of light extinction due to cohesive sediments in a shallow coastal lagoon under well mixed conditions. Sci. Total Environ. 694, 133707 https://doi.org/10.1016/j.scitotenv.2019.133707.

Verney, R., Lafite, R., Claude Brun-Cottan, J., Le Hir, P., 2011. Behaviour of a floc population during a tidal cycle: Laboratory experiments and numerical modelling. Cont. Shelf Res. 31, S64–S83. https://doi.org/10.1016/j.csr.2010.02.005.

Vowinckel, B., Withers, J., Luzzatto-Fegiz, P., Meiburg, E., 2019. Settling of cohesive sediment: particle-resolved simulations. J. Fluid Mech. 858, 5–44. https://doi.org/10.1017/jfm.2018.757.

Wang, Y.P., Voulgaris, G., Li, Y., Yang, Y., Gao, J., Chen, J., Gao, S., 2013. Sediment resuspension, flocculation, and settling in a macrotidal estuary. J. Geophys. Res. Ocean. 118, 5591–5608. https://doi.org/10.1002/jgrc.20340.

Winterwerp, J.C., 1998. A simple model for turbulence induced flocculation of cohesive sediment. J. Hydraul. Res. 36, 309–326. https://doi.org/10.1080/00221689809498621.

Ye, L., Manning, A.J., Holyoke, J., Penaloza-Giraldo, J.A., Hsu, T.-J., 2021. The role of biophysical stickiness on oil-mineral flocculation and settling in seawater. Front. Mar. Sci.

Yeung, A.K.C., Pelton, R., 1996. Micromechanics: a new approach to studying the strength and breakup of flocs. J. Colloid Interface Sci. 184, 579–585. https://doi.org/10.1006/jcis.1996.0654.

Zhang, J., Shen, X., Zhang, Q., Maa, J.P.-Y., Qiao, G., 2019. Bimodal particle size distributions of fine-grained cohesive sediments in a settling column with oscillating grids. Cont. Shelf Res. 174, 85–94. https://doi.org/10.1016/j.csr.2019.01.005.